Research in Astron. Astrophys. **2011** Vol. **11** No. **1**, 103–118
http://www.raa-journal.org *http://www.iop.org/journals/raa*

Research in Astronomy and Astrophysics

On some applications of invariant manifolds *

Xi-Yun Hou, Lin Liu and Yu-Hui Zhao

Astronomy Department, Nanjing University, Nanjing 210093, China; *silence@nju.edu.cn*
Institute of Space Environment and Astrodynamics, Nanjing University, Nanjing 210093, China

Received 2010 May 29; accepted 2010 July 26

Abstract Taking transfer orbits of a collinear libration point probe, a lunar probe and an interplanetary probe as examples, some applications of stable and unstable invariant manifolds of the restricted three-body problem are discussed. Research shows that transfer energy is not necessarily conserved when invariant manifolds are used. For the cases in which the transfer energy is conserved, the cost is a much longer transfer time.

Key words: celestial mechanics

1 INTRODUCTION

The Circular Restricted Three-Body Problem (CRTBP) is one of the most commonly used models in deep space exploration. It describes the motion of a massless small body P pulled by the gravitation of two massive primaries P_1 and P_2 which revolve around each other in circular orbits. We usually describe the motion of the massless small body in a coordinate which rotates with the two primaries, called the synodic coordinate (Szebehely 1967). The equation of motion of the small body cannot be solved in explicit analytic forms. There are five equilibrium points called libration points in the system. Three of them are called collinear libration points, lying on the line connecting the two primaries. Figure 1 shows the configuration of these three points, where C is the barycenter of the two primaries P_1 and P_2.

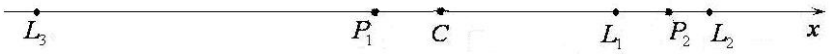

Fig. 1 Configuration of the three collinear libration points and the two primaries.

The collinear libration points are unstable but with conditionally stable motions around them. Their dynamics have already been carefully studied (Gómez et al. 2001a,b). Nowadays, these points are widely used in space missions due to their unique positions and dynamical characteristics. Generally, two types of applications exist. One type is to put a probe in conditionally stable orbits around these points (Farquhar & Kamel 1973), such as ISEE-3, SOHO and PLANCK. The other type is to utilize them as energy saving passages for the probes. This paper concentrates on the second type of application. The fundamental tools for this type of application are the associated stable and unstable invariant manifolds. For both the collinear libration points and the conditionally stable

∗ Supported by the National Natural Science Foundation of China.

orbits around them, there are stable and unstable invariant manifolds associated with them. These manifolds gradually extend into space, and can be used to guide the collinear libration probe (the probe which is located around the collinear libration points) as it approaches the Earth (Gómez et al. 1993). The manifolds can also be used as passages between different libration points in the same restricted three-body problem (Koon et al. 2000; Gómez et al. 1998) or between libration points in different restricted three-body problems (Koon et al. 2001; Franco et al. 2004). In these applications, connecting arcs can be used if the manifolds do not intersect in space (Franco et al. 2004). In the following, for brevity, when we talk about the invariant manifolds of the point L_i, we actually mean the invariant manifolds associated with the conditionally stable orbits around the point L_i.

Different from the traditional patched conic method (Battin 1999) used in the design of interplanetary transfer orbits, the patched manifold method (Lo 2002; Gómez et al. 2004) is based on stable and unstable invariant manifolds of the restricted three-body problem. In some cases, the transfer orbit designed by the patched manifold method requires less energy than the one designed by the patched conic method, but usually requires more transfer time. In some cases, the transfer orbit designed by the patched manifold method requires not only more time but also more energy than the one designed by the patched conic method.

Taking the transfer orbits of the collinear libration point probe, the lunar probe and the interplanetary probe as examples, applications of the invariant manifolds in deep space explorations are studied. For the results already obtained by previous works, we only briefly sketch them. Instead, we concentrate on the results which differ from the previous studies. The force models used in the paper are the CRTBP and the real force model. The real force model in our work includes gravitation of the Sun, the nine planets (including Pluto) and the Moon. Their positions are given by the JPL DE405 numerical ephemeris.

2 STABLE AND UNSTABLE INVARIANT MANIFOLDS

In the barycenter synodic coordinate, the dimensionless equation of motion of the small body follows (Szebehely 1967)

$$\begin{cases} \ddot{\boldsymbol{r}} + 2(-\dot{y}, \dot{x}, 0)^T = (\partial\Omega/\partial\boldsymbol{r})^T, \\ \Omega = (\mu(1-\mu) + x^2 + y^2)/2 + (1-\mu)/r_1 + \mu/r_2, \end{cases} \tag{1}$$

where $\boldsymbol{r}_1$, and $\boldsymbol{r}_2$ are position vectors of the small body from the two primaries. In addition, $\mu = m_2/(m_1+m_2)$, where m_1 and m_2 are the masses of the two primaries, and $m_2 < m_1$. An integral of Equation (1), called the Jacobi integral, exists in the form

$$2\Omega - v^2 = 2\Omega - (\dot{x}^2 + \dot{y}^2 + \dot{z}^2) = C\,, \tag{2}$$

where v is the speed of the small body. Expanding Equation (1) around the collinear libration points and only collecting the linear terms in the expansion, the linear solution of the motion around these points can be obtained in the form (Szebehely 1967)

$$\begin{cases} \xi = C_1 d^{d_1 t} + C_2 e^{-d_1 t} + C_3 \cos d_2 t + C_4 \sin d_2 t\,, \\ \eta = \alpha_1 C_1 d^{d_1 t} - \alpha_1 C_2 e^{-d_1 t} - \alpha_2 C_3 \cos d_2 t + \alpha_2 C_4 \sin d_2 t \quad , \\ \zeta = C_5 \cos d_3 t + C_6 \sin d_3 t\,, \end{cases} \tag{3}$$

where $\boldsymbol{\rho} = (\xi, \eta, \zeta)^T$ indicates the deviation of the small body from the corresponding collinear libration point. $C_1 \sim C_6$ are constants of motion determined by the initial state of the orbit. When $C_1 = C_2 = 0$, Equation (3) describes a conditionally stable orbit which is denoted as $\bar{\boldsymbol{\rho}}$. When $C_1 = 0$ and $C_2 \neq 0$, $\boldsymbol{\rho}$ asymptotically approaches $\bar{\boldsymbol{\rho}}$ with increasing t. These orbits are called asymptotically stable orbits. When $C_1 \neq 0$ and $C_2 = 0$, $\boldsymbol{\rho}$ asymptotically approaches $\bar{\boldsymbol{\rho}}$ with decreasing t. These orbits are called asymptotically unstable orbits. The set of asymptotic stable orbits

is called the stable invariant manifold and the set of asymptotically unstable orbits is called the unstable invariant manifold. Dynamically speaking, the conditionally stable orbit $\bar{\boldsymbol{\rho}}$ is also an invariant manifold. However, without special emphasis, the invariant manifolds in this paper indicate the stable or the unstable ones.

Considering higher order expansions of Equation (1), the conditionally stable orbit $\bar{\boldsymbol{\rho}}$ and its associated stable and unstable invariant manifolds still exist, with a form much more complicated than Equation (3). Regarding computations of these elements, readers are lead to Gómez et al. (2001a,b) for details.

When the small body is restricted to move in the $x - y$ plane, the CRTBP is reduced to the Planar Circular Restricted Three-Body Problem (PCRTBP). Since the PCRTBP is a two dimensional system, Poincaré sections can be employed to study its dynamical properties (Koon et al. 2001).

Figure 2 shows the invariant manifolds of the PCRTBP with mass parameters of the Sun-Earth system. The right frame is the local magnification of the left one. Usually, four Poincaré sections $U_1 \sim U_4$ are used, as indicated in Figure 2. The Poincaré sections of the invariant manifolds are homogeneous with regard to circles (Llibre et al. 1985). The left frame of Figure 3 shows the first section of U_2 for the stable and unstable invariant manifolds of the point L_2. The right frame shows the first section of U_2 for the stable invariant manifold of the point L_1 and the first section of U_2 for the unstable invariant manifold of the point L_2. The curves S and U in these frames indicate the stable and unstable invariant manifolds respectively. The points inside the curves S or U are the orbits which can pass the corresponding collinear libration point, while the points outside are the orbits which cannot. The intersection points of the two curves are the orbits which automatically evolve from the unstable manifold to the stable one (under the condition that the energies of the two manifolds are the same). For the intersection case, if the stable and unstable invariant manifolds are associated with the same collinear libration point, the intersection point indicates a homoclinic orbit. Otherwise, it indicates a heteroclinic orbit (Koon et al. 2000). For the points inside both curves S and U, they indicate the orbits which first pass the collinear libration point corresponding to the unstable manifold and then pass the collinear libration point corresponding to the stable manifold. Readers are referred to Koon et al. (2000) for more details of these sections. For the three-dimensional case, Poincaré sections cannot be directly used due to the Arnold diffusion. There is some research on this problem. Please see Gómez et al. (2004).

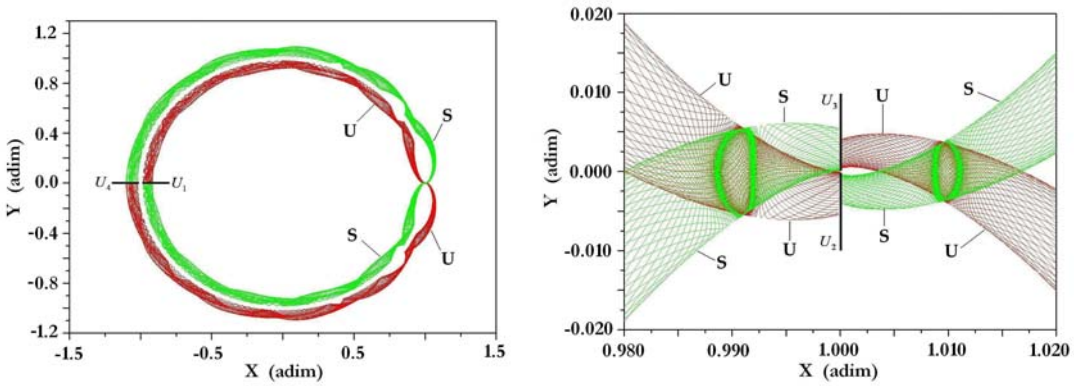

Fig. 2 Stable and unstable invariant manifolds of the collinear libration points in the Sun-Earth restricted three-body problem. Here "adim" in the labels indicates that the length unit is the mean distance between the Sun and the Earth.

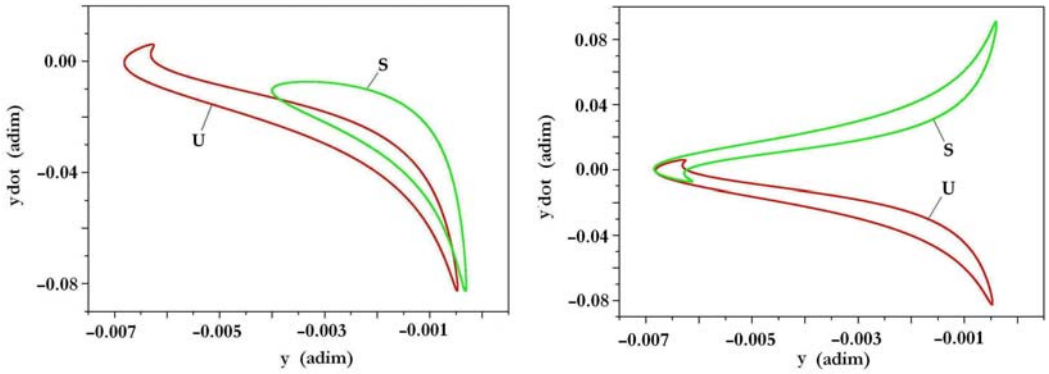

Fig. 3 Poincaré sections of the stable and unstable invariant manifolds of the section U_2 where "ydot" in the labels are actually $\dot{y}$. In addition, "adim" in the abscissa indicates that the length unit is the mean distance between the Sun and the Earth, and "adim" in the ordinate indicates that the velocity unit is 29784.7365615637 m s^{-1}.

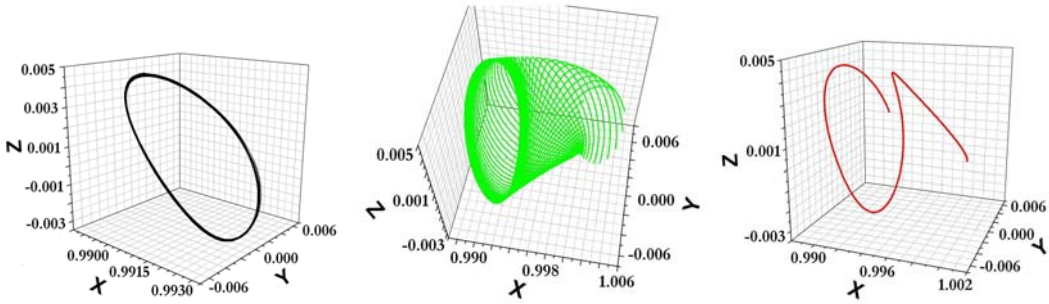

Fig. 4 *Left:* the nominal orbit of the probe; *Middle:* the stable invariant manifold associated with the nominal orbit; *Right:* a chosen transfer orbit. The length unit of all three figures is the mean distance between the Sun and the Earth.

The heteroclinic orbits can be used as automatic transfer orbits between different collinear libration points. They have already been used in the GENESIS mission (Lo et al. 1998). We will not discuss such applications in the paper. The results in Figures 2 and 3 are all about the points L_1 and L_2. For the point L_3, its instability is very mild, and its associated stable and unstable invariant manifolds require a prohibitively long time to escape the proximity of the point L_3 and cannot approach the two primaries. Usually, we do not consider using the invariant manifolds associated with the point L_3.

3 COLLINEAR LIBRATION POINT PROBE

These probes should stay around the collinear libration points for a long time. Usually, the conditionally stable orbits (Lissajous orbits or Quasi-Halo orbits) around the collinear libration points are used as nominal orbits for these probes. The stable invariant manifolds associated with these nominal orbits can be used to guide the probes.

3.1 The Sun-Earth+Moon System

For the conditionally stable orbits with large energy around the points L_1 or L_2 in the Sun-Earth+Moon system, their stable manifolds can approach the Earth. If these manifolds intersect a parking Low Earth Orbit (LEO), a maneuver at the intersection point can send the probe from the LEO to the stable invariant manifolds. Then the probe automatically evolves into the nominal orbit. We usually choose the asymptotic stable orbit satisfying the following conditions to be the transfer orbit.

$$\boldsymbol{r}_{\rm e} \cdot \dot{\boldsymbol{r}}_{\rm e} = 0, \qquad r_{\rm e} - a_{\rm e} = h_{\rm LEO}\,, \tag{4}$$

where $\boldsymbol{r}_{\rm e}$ and $\dot{\boldsymbol{r}}_{\rm e}$ are the position and speed vectors of the probe from the Earth, $a_{\rm e}$ is the equatorial radius of the Earth and $h_{\rm LEO}$ is the height of the circular parking LEO. Of course, other restrictions may exist when designing a transfer orbit. Nevertheless, to simplify the problem, we only consider the restrictions of Equation (4).

Figure 4 shows a conditionally stable orbit (a Quasi-Halo orbit) around the point L_1 in the real force model (left frame), its associated stable invariant manifolds (middle frame) and the chosen transfer orbit (right frame). Here $h_{\rm LEO} = 200$ km. The maneuver at the LEO is 3196.53 m s^{-1} and the transfer time is 232.6 d. If lunar gravity assist can be used, more transfer energy can be saved (Liu et al. 2007).

Such transfer orbits usually require a very long transfer time (about 200$\sim$300 d). In addition, the stable invariant manifolds cannot approach the Earth if the energy of the nominal orbit is small. A two-maneuver strategy was proposed (Hou & Liu 2008). The two maneuvers are done in the parking LEO and in the nominal orbit respectively. With this strategy, transfer to the nominal orbit using small energy is possible and the transfer orbit requires much less time at the cost of slightly more energy.

3.2 The Earth-Moon System

We first consider the probes around the point L_1. For the PCRTBP of the Earth-Moon system, the stable invariant manifolds of the point L_1 cannot approach the Earth very closely (Koon et al. 2000). For the three-dimensional case and the real force model, a similar phenomenon happens, although it cannot be proven theoretically. Studies show that for energy "openings" close to C_{L_1} (where C_{L_1} is the Jacobi constant of the point L_1), the minimum distance between the stable manifolds and the Earth is about one tenth of the mean distance between the Earth and the Moon, i.e. about 38 000 km. As a result, for LEOs with height less than 38 000 km-a_e, it is not possible for the stable invariant manifolds to intersect them. A connecting arc is necessary, as shown in Figure 5. P is on the parking LEO and Q is on the stable invariant manifold. Denote the maneuver at P as Δv_1 and the maneuver at Q as Δv_2. Varying P, Q and the energy of the nominal orbit (i.e. the energy of the stable invariant manifold), the minimum of $\Delta v_1 + \Delta v_2$ can be obtained. The left frame of Figure 6 shows such an optimized transfer orbit to a Halo orbit around the point L_1 in the CRTBP model. For clarity, only the $x - y$ projection is given. The connecting arc PQ lasts 3.67 d and the asymptotic stable arc lasts 91.44 d. Here, $\Delta v_1 = 3109.13$ m s^{-1}, $\Delta v_2 = 420.95$ m s^{-1} and $h_{\rm LEO} = 200$ km. The minimum energy of a direct transfer orbit to the nominal orbit is about the same value (Alessi et al. 2010).

For the probe around the point L_2, the heteroclinic orbit between the conditionally stable orbits around the points L_1 and L_2 can be used. The transfer energy is approximately the same as the case of the point L_1. The right frame of Figure 6 shows such an optimized transfer orbit to a Halo orbit around the point L_2 in the CRTBP model. The connecting arc PQ lasts 3.49 d and the asymptotic stable arc lasts 99.62 d. Here $\Delta v_1 = 3105.36$ m s^{-1}, $\Delta v_2 = 451.23$ m s^{-1}, and $h_{\rm LEO} = 200$ km.

The minimum energies of the transfer orbits given here are similar to the ones in Alessi et al. (2010), but much larger than the ones given in Franco et al. (2004). From the analysis for the lunar probe below, we speculate that the results of Franco et al. (2004) should be doubted.

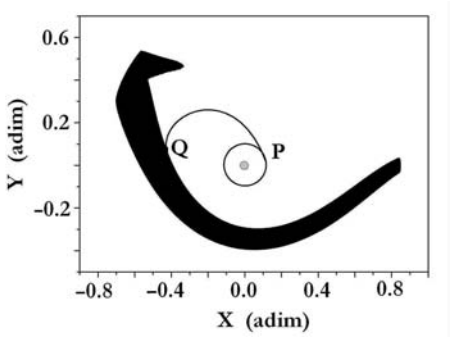

Fig. 5 An illustration depicting the connecting arc and the stable invariant manifold of the point L_1 in the Earth-Moon system.

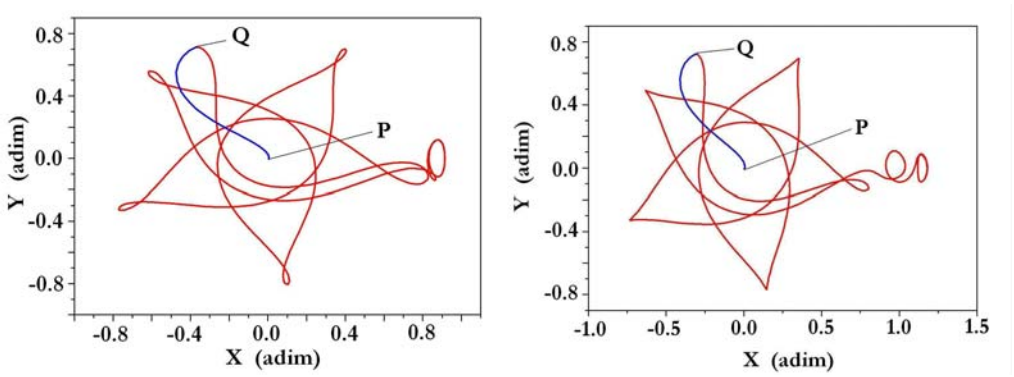

Fig. 6 *Left:* A transfer orbit to a Halo orbit around the point L_1 in the Earth-Moon system ($x-y$ projection); *Right:* A transfer orbit to a Halo orbit around the point L_2 in the Earth-Moon system ($x-y$ projection). Here "adim" in the labels indicates that the length unit is the mean distance between the Earth and the Moon.

A note should be made here. Although the stable invariant manifolds of the point L_1 in the Earth-Moon system cannot approach the Earth very closely, they can approach the Moon very closely (similar to the right frame of Figure 2 for the Sun-Earth system). As a result, if the second maneuver of the connecting arc is around the Moon, the minimum transfer energy can be saved compared with the results above (Lo & Chung 2002). Readers can refer to the reference for more details.

3.3 The Optimization Scheme

For the transfer orbit in Figure 4 of the Sun-Earth+Moon system, optimization is not needed. The minimum distance of different asymptotic stable orbits on the stable invariant manifold can be obtained from the first equation of Equation (4). We simply choose the one which satisfies the second equation of Equation (4) as the transfer orbit.

For the orbits in Figure 6 in the Earth-Moon system, optimization is done like this. Take the halo orbit around the point L_1 as an example. We first divide the halo orbit into N parts. The time interval of each part is the same. Denote the nodal points on the halo orbit as $i = 1 \sim N$. For each nodal

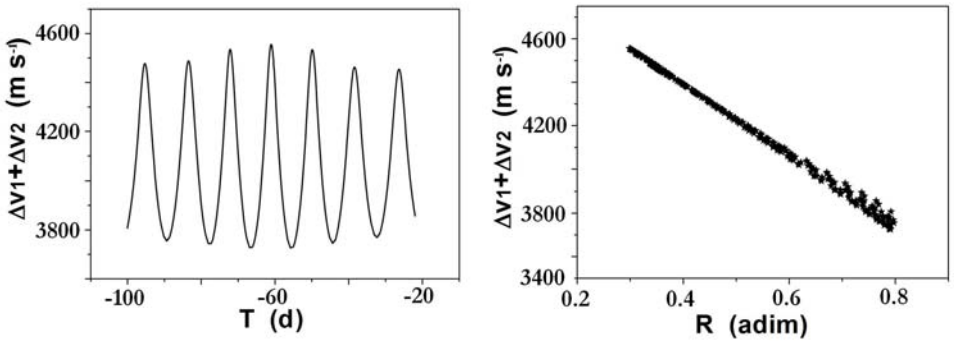

Fig. 7 *Left:* the curve of $\Delta v_1 + \Delta v_2$ with respect to different points Q in one asymptotic orbit; *Right:* distribution of $\Delta v_1 + \Delta v_2$ with respect to the distances of different points Q from the Earth. Here "adim" in the label of the right figure indicates that the length unit is the mean distance between the Earth and the Moon.

point, we compute the corresponding asymptotically stable orbit and integrate it backwards to the point Q. Then we compute the speed corrections at the points P (denoted as Δv_1) and Q (denoted as Δv_2). To simplify the computations, the point Q is transferred from the synodic frame to the sidereal frame. The connecting arc PQ is taken as a part of an ellipse whose perigee and apogee are the points P and Q respectively. Then Δv_1 and Δv_2 can be computed immediately for each point Q on the stable invariant manifold. For clarity, we pick one asymptotic orbit as an example to show the curve of $\Delta v_1 + \Delta v_2$, as shown in Figure 7. The abscissa of the left figure is the integration time of the asymptotic orbit. The abscissa of the right figure is the minimum distance of the point Q from the Earth. Clearly, the minimum values of energy correspond to the points Q which are furthest from the Earth.

It is unnecessary for N to be very large. A modest number (say 100) is enough. Suppose the minimum energy corresponds to a point Q on one asymptotic stable orbit which is associated with the nodal point J on the halo orbit. Then we divide the parts of the halo orbit from the nodal point $J-1$ to $J+1$ into N smaller parts and do the optimization process again. The process stops when the step of the nodal points is smaller than a threshold. By doing this, we can gradually approach the optimized value. For the transfer orbits to the halo orbit around the point L_2, the optimization process is the same, but those cases are restricted to the asymptotic orbits which can approach the Earth through the heteroclinic connections with the point L_1.

Since the true connecting arc PQ, of course, is not part of a fixed ellipse, the optimal transfer orbit found by the above scheme is not the true optimal transfer orbit in the real force model. However, the deviation between the two is very small because the two-body problem is a good approximation for the arc PQ. The deviation of the total energy is usually within $10\,\mathrm{m\,s^{-1}}$.

4 LUNAR PROBE

The traditional Hohmann transfer orbit of a lunar probe requires about 2∼5 d, with two maneuvers in the parking LEO and in the nominal orbit respectively. The second maneuver of such a transfer orbit is necessary because the orbit is hyperbolic when the probe enters the gravitational sphere of the Moon. However, the transfer orbit designed by the patched manifold method is elliptic when the probe enters the Moon's gravitational sphere. As a result, the second maneuver is unnecessary.

4.1 Through the L_1 Point

As stated in the above section, the orbits inside the Poincaré sections of the stable invariant manifolds can pass the corresponding collinear libration point. Such orbits are called transferable orbits. They are the orbits used to guide the lunar probe. Since all the transferable orbits are enveloped by the invariant manifolds, they cannot approach the Earth very closely. Similar to Figure 5, a connecting arc is necessary. The difference is that Q is in the transferable orbits instead of the stable invariant manifold. Varying the positions of P, Q and the stable invariant manifold, a transfer orbit with minimum energy can be found.

Figure 8 shows such an optimized transfer orbit in the CRTBP model. The connecting arc PQ requires 3.33 d. From Q to the point L_1 requires 362.85 d. Here $\Delta v_1 = 3102.11\,\mathrm{m\ s^{-1}}$, $\Delta v_2 = 393.93\,\mathrm{m\ s^{-1}}$ and $h_{\mathrm{LEO}} = 200\,\mathrm{km}$. The right frame shows the trajectory of the probe after passing through the point L_1, lasting about one year.

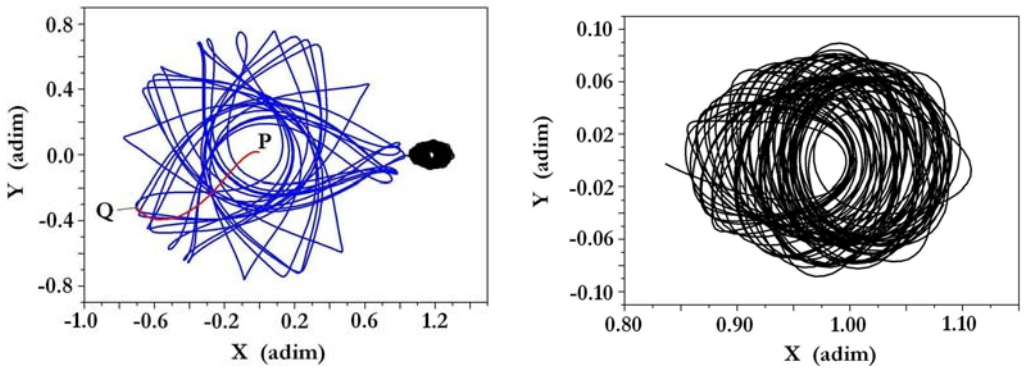

Fig. 8 A transfer orbit to the Moon through the L_1 point where "adim" in the labels indicates that the length unit is the mean distance between the Earth and the Moon.

We can estimate the minimum energy needed for such transfer orbits. Viewed from an Earth centered sidereal coordinate, the stable invariant manifolds are actually precessing ellipses with very large eccentricities. Studies show that the transfer energy is close to minimum when Q is at the apogee of these ellipses (Alessi et al. 2010), a conclusion in accordance with Figures 6 and 7. Since the height of the LEO is fixed, the transfer energy is determined by the perigee and apogee of the ellipses. The ellipses are precessing, thus the perigee and apogee are not fixed. Studies show that the apogee is around eight tenths of the mean distance between the Earth and the Moon. Variations of the exact values will not affect the total energy very much. The transfer energy is mainly determined by the perigee. Obviously, the energy is smaller for a smaller perigee. As stated above, the minimum value of the perigee is about one tenth of the mean distance between the Earth and the Moon. If the height of the LEO is h_{LEO} =200 km, then the minimum energy needed is around $\Delta v = \Delta v_1 + \Delta v_2$ =3162.07 +320.95 =3465.03 (m s^{-1}). This value is close to the one in Figure 8 but much larger than the one in Franco et al. (2004). It is not quite possible to transfer an orbit with energy much less than this value. As a result, we speculate that the results in Franco et al. (2004) should be doubted. Similarly, the results of a transfer to the conditionally stable orbit around the points L_1 and L_2 should also be doubted.

Compared with the Hohmann transfer method, transfer through the L_1 point requires less energy if no requirements are made on the nominal orbit. However, if the nominal orbit of such a transfer orbit is required to be the same as the Hohmann transfer, the conclusion is different. Suppose the

height of the parking LEO is 200 km and the height of the nominal orbit around the Moon is 100 km. The energy of a typical Hohmann transfer orbit is about 4000 m s^{-1}. For the transfer orbit through the L_1 point, a third maneuver Δv_3 is required to insert the probe into the nominal orbit. Usually, the orbit is highly elliptic (very close to 1) when the probe enters the Moon's gravitational sphere. Approximately, we can take it as a parabolic orbit. Suppose the height of the perilune is 100 km, then the maneuver Δv_3 to insert the probe into the nominal orbit is about 676.51 m s^{-1}. The minimum total energy needed is around $\Delta v = \Delta v_1 + \Delta v_2 + \Delta v_3$ =4141.54 m s^{-1}, which is a value larger than that of the Hohmann transfer orbit. Since transfer through the L_1 point requires more energy and time than the Hohmann transfer, it is not an ideal way to guide the lunar probe.

4.2 Through the L_2 Point

Generally, the stable invariant manifolds of the point L_2 in the CRTBP can only approach the Earth by passing through the point L_1. However, in the real force model, due to the Sun's perturbations, the probe can first go beyond the point L_2 of the Earth-Moon system via the stable and unstable invariant manifolds of the Sun-Earth system and then enter the Moon's gravitational region via the stable invariant manifolds of the point L_2 of the Earth-Moon system. The left frame of Figure 9 is an illustration depicting the mechanism. The right frame shows such a transfer orbit in the Earth centered sidereal coordinate ($x - y$ projection). The starting epoch is MJD=54457.00. The transfer time is 102.04 d. The first maneuver at the parking LEO is 3200.07 m s^{-1}, and the second maneuver at the nominal orbit is 647.63 m s^{-1}. The heights of the LEO and the nominal orbits are both 200 km.

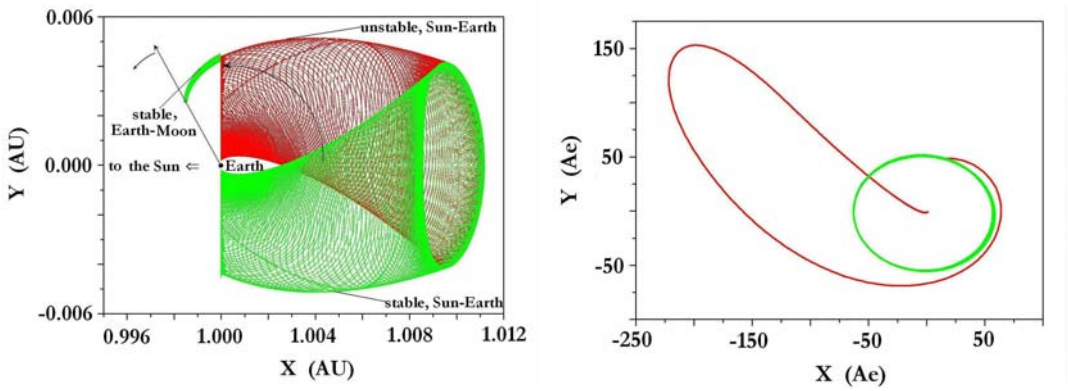

Fig. 9 *Left:* An illustration depicting the intersection between the stable invariant manifold of the Earth-Moon system and the stable and unstable invariant manifolds of the Sun- Earth system. *Right:* An example WSB transfer orbit, with the circle indicating the Moon's orbit. "AU" in the left frame indicates the length unit to be the astronomical unit, and "Ae" in the right frame indicates the length unit to be the equatorial radius of the Earth.

Such transfer orbits were first obtained by Belbruno (Belbruno 1987). Then Koon et al. explained their dynamics (Koon et al. 2001). These orbits are often referred to as lunar ballistic trajectories or Weak Stability Boundary (WSB) trajectories. Regarding the ways to find such orbits, readers can refer to Circi & Teofilatto (2001). Generally, such transfer orbits require less energy than the Hohmann transfer orbits, but with a much longer transfer time. They can only be used in missions with no requirements for the transfer time.

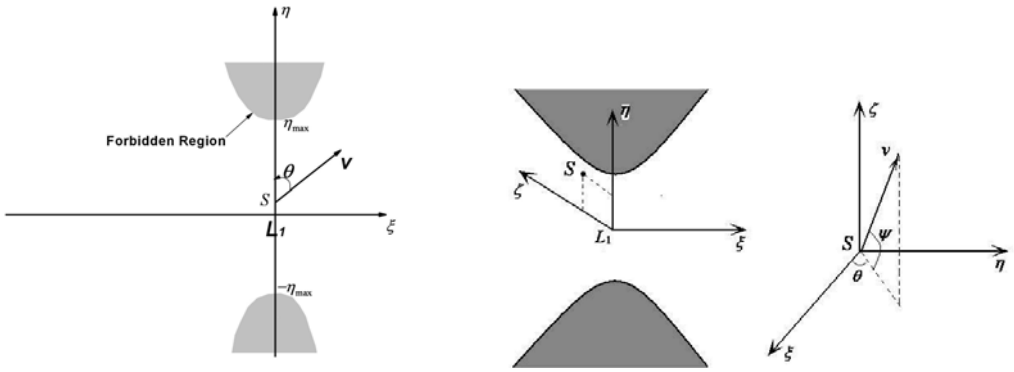

Fig. 10 Illustrations depicting the optimization scheme. Left is for the planar case. Right is for the three dimensional case.

4.3 The Optimization Scheme

Compared with the optimization problem in Subsection 3.3, there are two differences in the optimization of the transfer orbits of the lunar probe through the L_1 point. First, the energy of the stable manifold is not fixed because no specific requirements are made on the conditionally stable orbits around the point L_1. Second, the orbits we are studying are in fact the transferrable orbits enveloped by the stable invariant manifolds, which can pass the point L_1. Optimization can be done as follows. First, we fix the energy of the conditionally stable orbit around the point L_1 and compute the transfer orbits. Then the energy of the conditionally stable orbit is varied to find the global optimal transfer orbit.

In our optimization process, however, we did not compute the conditionally stable orbits. Since all the transfer orbits should pass the point L_1, they can be computed like this. Taking the planar case as an example, for a Jacobi constant C slightly smaller than C_1, the opening neck (the region between the two forbidden regions in Fig. 10) around the point L_1 is small (Szebehely 1967). Denote the intersection point of the transfer orbit with the η axis as S. The speed at the point S has angle θ with respect to the η axis. We then integrate forwards and backwards from the point S. If the probe is captured by the Earth when integrating backwards and captured by the Moon when integrating forwards, then this indicates a transfer orbit has been found. Varying the η coordinate of the point S and its speed direction angle θ, and varying the Jacobi constant C, we can find the transfer orbit with the minimum transfer energy.

Denote the smallest Jacobi constant we studied as $C_{\min}$. First, we divide the interval $[C_{\min}, C_1]$ into N_1 parts. For each Jacobi constant $C_i = C_{\min} + (C_1 - C_{\min}) \times i/N_1$, the $\eta_{\max}$ in Figure 10 can be obtained. For the coordinate η of the point S, we divide the interval $[-\eta_{\max}, \eta_{\max}]$ into N_2 parts, and for the angle θ, we divide the interval $[0^\circ, 360^\circ]$ into N_3 parts. First, we fix the values of N_2 and N_3 (say 100). For a modest value of N_1 (say 100), the optimal transfer orbit can be obtained. Suppose this process happens for the Jacobi constant C_J. Then we divide the interval C_{J-1} to C_{J+1} into N_1 parts again to renew the optimization process. When the step of the Jacobi constant is smaller than a threshold (say 10^{-8}), we fix the Jacobi constant. Suppose, for this fixed Jacobi constant, the optimal transfer orbit happens for $\eta_K = -\eta_{\max} + 2K\eta_{\max}/N_2$ and $\theta_L = 360^\circ L/N_3$. We divide the interval $[\eta_{K-1}, \eta_{K+1}]$ into N_2 parts and the interval $[\theta_{L-1}, \theta_{L+1}]$ into N_3 parts to iterate the optimization process. The whole optimization process stops when the steps of η and θ are smaller than a threshold.

Similar to the case in Subsection 3.3, the point Q is transferred from the synodic frame to the sidereal frame and the connecting arc PQ is taken as a part of a fixed ellipse to save computation time. When the optimal value is found, the arc PQ is numerically refined to obtain the true transfer orbit. For the three-dimensional case, a similar optimization process can be applied, as shown in the right frame of Figure 10. However, the process is more complicated because of two additional components ζ and $\dot{\zeta}$. The results in Figure 9 correspond to the planar case.

For the WSB transfer orbit, there are already many studies which have been published, so there is no need to discuss it further in this paper.

5 INTERPLANETARY PROBE

The traditional method to design an interplanetary trajectory is the patched conic method (Battin 1999). The trajectory can be computed by patching many conic sections together. Take the Mars probe as an example. The transfer trajectory from the Earth can be taken as three conic sections patched together: the geocentric hyperbolic arc, the areocentric hyperbolic arc and the heliocentric Lambert arc. These conics are first patched together geometrically and then numerically refined to obtain a true transfer orbit in the real force model.

Different from the patched conic method, the patched manifold method is based on stable and unstable invariant manifolds of the CRTBP. Take those paths departing from the Earth as an example. When the nominal planet is within the orbit of the Earth, the probe first escapes from the Earth via the unstable invariant manifolds of the point L_1 in the Sun-Earth system and then approaches the nominal planet via the stable invariant manifolds of the point L_2 in the Sun-nominal planet system. When the nominal planet is outside the Earth's orbit, the probe first escapes from the Earth via the unstable invariant manifolds of the point L_2 in the Sun-Earth system and then approaches the nominal planet via the stable invariant manifolds of the point L_1 in the Sun-nominal planet system. According to the calculation of intersections between the two invariant manifolds, we study the problem in two cases and compare the result with the orbit designed by the patched conic method.

5.1 The Case of No Intersections

For the CRTBPs composed of the Sun and the terrestrial planets, their invariant manifolds cannot intersect (Lo 2002). As a result, a connecting arc is necessary to fulfill the transfer between the two manifolds. Taking a Mars probe from the Earth as an example, the connecting arc links the unstable invariant manifold of the point L_2 in the Sun-Earth system with the stable invariant manifolds of the point L_1 in the Sun-Mars system. There are totally four maneuvers in the transfer orbit: At the epoch T_1, the first maneuver Δv_1 sends the probe from the parking LEO to the unstable invariant manifold of the Sun-Earth system; At the epoch T_2, the second maneuver Δv_2 at one end of the connecting arc (denoted as P) sends the probe to the connecting arc; At the epoch T_3, the third maneuver Δv_3 at the other end of the connecting arc (denoted as Q) sends the probe to the stable invariant manifold of the Sun-Mars system; At the epoch T_4, the last maneuver Δv_4 inserts the probe into the nominal orbit. The configuration of the two restricted three-body problems and their invariant manifolds are shown in the left frame of Figure 11. The angle θ is the angle between the Sun-Earth system at the epoch T_2 and the Sun-Mars system at the epoch T_3.

Assume the orbits of the Earth and Mars are coplanar circular orbits. The initial phase angle can be given by the ephemeris. Four steps are taken to find such transfer orbits:

(1) Compute the unstable invariant manifold of the point L_2 in the Sun-Earth system and compute the stable invariant manifold of the point L_1 in the Sun-Mars system.
(2) Pick two ends of the connecting arc PQ at the two invariant manifolds. Set the epoch T_2 at P and the epoch T_3 at Q, then the angle θ in Figure 11 can be obtained. Neglecting the gravitation of the Earth and Mars, the heliocentric Lambert arc PQ is solved.

(3) According to the restrictions of the parking LEO, the Earth leg, which connects the point P with the parking LEO, is solved. Similarly, the Mars leg, which connects the point Q with the nominal orbit, is solved. Along with the heliocentric arc PQ, the four maneuvers $\Delta v_1, \Delta v_2, \Delta v_3$ and Δv_4 can be obtained.
(4) Vary the invariant manifolds and the positions of P and Q on the manifolds and the epochs T_2 and T_3 to find the minimum of $\Delta v_1 + \Delta v_2 + \Delta v_3 + \Delta v_4$. Numerically refine this orbit to find the true transfer orbit in the real force model.

The right frame of Figure 11 shows such an optimized transfer orbit in the heliocentric celestial frame. The height of the parking LEO is 200 km and the height of the nominal orbit is 500 km. The four maneuvers are Δv_1=3211.93, Δv_2=2659.78, Δv_3 =2334.01 and Δv_4 =1399.92 m s^{-1}. The Earth leg requires 248.39 d, the heliocentric Lambert arc requires 350.00 d and the Mars leg requires 331.10 d. The epoch T_2 is MJD=55847.5.

Compared with the transfer orbit designed by the patched conic method (with minimum energy around 5735.00 m s^{-1} and transfer time around 300 d), a transfer orbit designed by the patched conic method requires more energy and more time. Of course, transfer orbits with less transfer energy than that of the Figure 11 might exist, but generally the conclusion is the same: they require more energy and time than the best transfer orbit designed by the patched conic method. This phenomenon can be explained. The invariant manifolds of the Sun-Earth system and the Sun-Mars system are actually precessing ellipses in a heliocentric sidereal coordinate. Denote their semi-major axes as a_1 and a_2. Generally, $a_1 > a_{\rm Earth}$ and $a_2 < a_{\rm Mars}$. As a result, $\Delta v_2 + \Delta v_3$ is smaller than the total energy of the transfer orbit designed by the patched conic method. However, sending the probe from the parking LEO to the unstable invariant manifold and inserting the probe to the nominal orbit from the stable invariant manifold require two additional maneuvers Δv_1 and Δv_4. The sum of $\Delta v_1, \Delta v_2, \Delta v_3$ and Δv_4 is larger than that of the transfer orbit designed by the patched conic method. In order to make Δv_1 and Δv_4 as small as possible, the heights of the parking orbits and the nominal orbits should be very large. That explains why the numerical examples in Franco et al. (2004) all have very high parking orbits and nominal orbits. Considering the energy needed to lift the height of the Earth parking orbit and lower the height of the nominal orbit, we do not recommend sending the probe via the invariant manifolds. The discussions and conclusions are not only valid for the Mars probe, but also valid for all the transfer orbits between the terrestrial planets.

5.2 The Case of Intersections

For the CRTBPs composed of the Sun and the Jovian planets, their invariant manifolds can intersect in space (Lo 2002). Take the transfer of a probe from Jupiter to Saturn as an example. The invariant manifolds are shown in the left frame of Figure 12. Since we are dealing with two different restricted three-body problems, the Poincaré sections of the two manifolds are given in a heliocentric sidereal coordinate. The Jacobi constant of the unstable invariant manifold is $C_1 = 3.02$, and the Jacobi constant of the stable invariant manifold is $C_2 = 3.01$. $\theta_1 = 5\pi/6$ and $\theta_2 = 5\pi/6$.

Figure 13 shows the Poincare section of the two manifolds. The units in Figure 13 are dimensionless units in the Sun-Jupiter system. In Figure 13, $R_d = \dot{R}$ is the radial speed and $R_v = |\dot{\boldsymbol{R}} - \dot{R}\boldsymbol{R}/R|$ is the transverse speed.

We tried to search for the points which simultaneously satisfy $R^{\rm Unstable} = R^{\rm Stable}$, $R_d^{\rm Unstable} = R_d^{\rm Stable}$ and $R_v^{\rm Unstable} = R_v^{\rm Stable}$ for different Poincaré sections (even for very large θ_1 and θ_2) and different invariant manifolds, but with no results. Seemingly no orbit can transfer from the unstable invariant manifolds of the Sun-Jupiter system automatically to the stable invariant manifolds of the Sun-Saturn system. As a result, a maneuver is needed at the intersection point to help carry out the transfer. There are totally three maneuvers in the transfer. The first maneuver Δv_1 sends the probe from the low Jupiter parking orbit to the unstable invariant manifold; The second maneuver Δv_2 sends the probe from the unstable invariant manifold of the Sun-Jupiter system to the stable

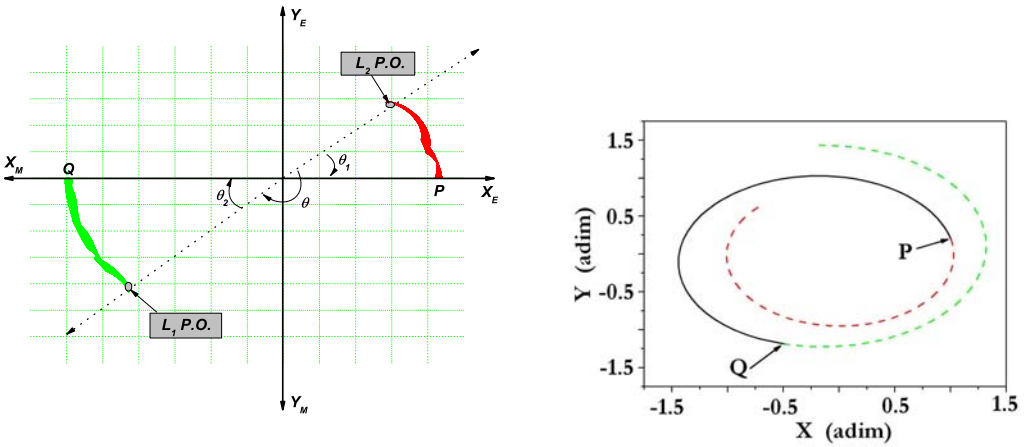

Fig. 11 *Left:* The configuration of the Sun-Earth system and the Sun-Mars system; *Right:* A Mars transfer orbit from the Earth utilizing the invariant manifolds ($x - y$ projection). Here "adim" in the labels indicates that the length unit is the astronomical unit.

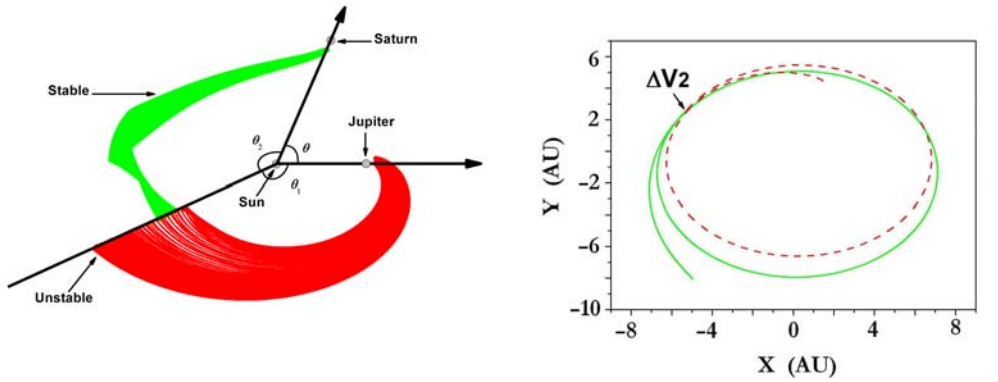

Fig. 12 *Left:* the configuration of the Sun-Jupiter system and the Sun-Saturn system and their invariant manifolds. *Right:* A transfer orbit from Jupiter to Saturn utilizing the invariant manifolds ($x - y$ projection). "AU" in the labels indicates that the length unit is the astronomical unit.

invariant manifold of the Sun-Saturn system; The third maneuver Δv_3 inserts the probe into the nominal low Saturn orbit. Of course, automatic transfer orbits may exist and we are simply unable to find them. However, even if these orbits do exist, they require a very long transfer time which is not ideal for practical use. In the paper, we only concentrate on the case $\Delta v_2 \neq 0$.

We choose the intersection point satisfying

$$R^{\text{Unstable}} = R^{\text{Stable}}, \qquad \min[(R_d^{\text{Unstable}} - R_d^{\text{Stable}})^2 + (R_v^{\text{Unstable}} - R_v^{\text{Stable}})^2] \tag{5}$$

as the transfer orbit candidate and numerically refine it to obtain the true transfer orbit in the real force model. Considering the facts that the orbits of Jupiter and Saturn are not coplanar and not circular, the orbit satisfying Equation (5) is not the true transfer orbit with minimum energy. Nevertheless,

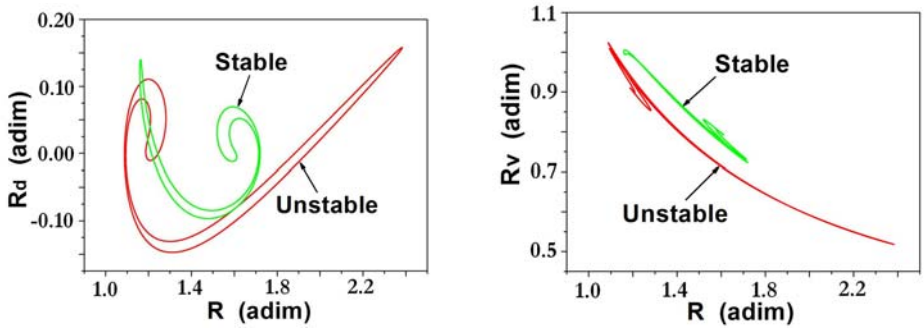

Fig. 13 Poincaré sections of the two invariant manifolds. The sections are given in a heliocentric sidereal coordinate. Here "adim" in the abscissa indicates that the length unit is the mean distance between the Sun and Jupiter. R_d in the labels are in fact $\dot{R}$, and "adim" in the ordinate indicates that the velocity unit is 13063.4618377826 m s^{-1}.

the energy of the transfer orbit designed by the algorithm above is close to the minimum value. The right frame of Figure 12 shows the transfer orbit. The height of the parking orbit is 500 000 km and the height of the nominal orbit is 400 000 km. Here $\Delta v_1 = 6063.43$, $\Delta v_2 = 1346.53$, and $\Delta v_3 = 4036.00$ m s^{-1}. The total speed is 11445.96 m s^{-1}. The time of the Jupiter leg is 7106.93 d and the time of the Saturn leg is 8719.87 d. The epoch at the intersection point is MJD=59152.50. Compared with the best transfer orbit designed by the patched conic method (with minimum energy around 10 100.00 m s^{-1} and transfer time around 4200 d), the orbit in Figure 12 also requires more transfer time and energy. As stated above, the orbits satisfying $\Delta v_2 \to 0$ might exist, but the energy saved is limited and the transfer time will be much longer than the one in Figure 12.

5.3 The Optimization Scheme

For the Mars probe, the optimization process is fulfilled like this. First we parameterize the two invariant manifolds. For each manifold, three parameters C_i, s_i and $\theta_i (i = 1, 2)$ are needed. C_i indicates the energy of the manifold, s_i indicates the exact asymptotic orbit on the manifold and θ_i indicates the geometrical position of the point P or Q on the manifold. Two additional parameters T_2 and T_3 are needed to fix the angle θ in Figure 11. So there are totally eight parameters in the optimization process. Even if the search region of each parameter is divided into 10 parts, there are 10^8 nodal points to be calculated. At each nodal point, we have to numerically integrate and refine the transfer orbit in the real force model to obtain Δv_1, Δv_2, Δv_3 and Δv_4. Obviously, the computation time is prohibitively large.

Studies show that the total energy is mainly affected by $\Delta v_2 + \Delta v_3$. As a result, to save the computation time, we did not compute the Earth leg and the Mars leg which consume most of the computation time. In addition, for the heliocentric arc, the two-body Lambert problem is used to obtain an approximation of $\Delta v_2 + \Delta v_3$. We take the minimum of $\Delta v_2 + \Delta v_3$ to be the candidate of the optimized transfer orbit and numerically refine it to obtain the true transfer orbit. Although the refined orbit is not the true optimal transfer orbit, it should be close to it. For an unstable manifold with energy C_1=3.00048668563031 and a stable manifold with energy C_2=3.00010342287611, with θ_1 and θ_2 varying from 0° to 180°, and the interval between the two epoches T_2 and T_3 varying from 100 d to 400 d, Figure 14 shows the time history of $\Delta v_2 + \Delta v_3$ with respect to the epoch T_2. For each invariant manifold, 20 asymptotic orbits are computed. The intervals of the angles θ_1 and θ_2 are divided into 180 parts. The step of the epoches T_2 and T_3 are 10 d. Similar to the Hohmann transfer

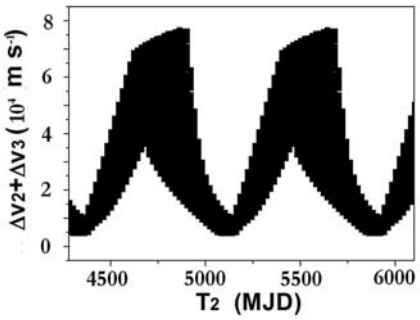

Fig. 14 Variation curve of $\Delta v_2 + \Delta v_3$ with respect to the epoch T_2.

orbit, an approximate 2-year launch window exists. Similar to the above cases, we can narrow the steps of the nodal points in the optimal transfer orbit to obtain a better result.

For the Saturn probe approaching from Jupiter, the optimization was not done. We choose the intersection point satisfying Equation (5) as the candidate of the transfer orbit. Generally, for invariant manifolds with larger energy and larger θ_1 and θ_2 values, the energy of the transfer orbit satisfying Equation (5) is smaller. However, much longer transfer times are needed due to larger θ_1 and θ_2 values.

A note should be made. The intersection point satisfying Equation (5) should be numerically refined to obtain the true transfer orbit in the real force model. Since the orbits of Saturn and Jupiter are elliptic and not in the same plane, the optimized transfer orbit in the two patched restricted three-body model is not the optimized transfer orbit in the real force model.

6 CONCLUSIONS

Taking the transfer orbits of the collinear libration point probe, the lunar probe and the interplanetary probe as examples, applications of the invariant manifolds in deep space explorations are discussed. Research shows that utilizing the invariant manifolds is not guaranteed to save energy, but will always cost more energy.

For the collinear libration point probe in the Sun-Earth system, the energy can be saved at the cost of more transfer time. A two maneuver strategy can save the transfer time greatly at the cost of slightly more energy. For the Earth-Moon system, the energy is about the same when utilizing the invariant manifolds as compared to sending the probe directly to the nominal orbit around the collinear libration points.

For the lunar probe with the same restrictions on the parking LEO and the nominal orbit, utilizing the stable invariant manifold of the point L_1 requires more transfer time and energy than the traditional Hohmann transfer orbit, thus it is not an ideal way to send the lunar probe. Utilizing the stable invariant manifolds of the point L_2 along with the invariant manifolds of the Sun-Earth system, the transfer energy can be saved, but at the cost of more transfer time.

For the interplanetary probe, in the case of no intersections between the invariant manifolds of the two restricted three-body problems, the transfer orbit designed by the patched manifold method requires more transfer time and energy than the one designed by the patched conic section method, and thus is not ideal for practical use. For the case of intersections, the transfer energy might be saved if $\Delta v_2 \to 0$, but at the cost of more transfer time.

Different optimization methods may give better results than the ones given in the paper, but the conclusions above still apply.

Acknowledgements This work was funded by the National Natural Science Foundation of China (Grant Nos. 10903002, 40974019).

References

Alessi, E. M., Gómez, G., & Masdemont, J. 2010, Advances in Space Research, 45, 1276
Battin, R. H. 1999, An Introduction to the Mathematics and Methods of Astrodynamics, Revised ed., (Reston: American Institute of Aeronautics and Astronautics, Inc.)
Belbruno, E. A. 1987, AIAA, DGLR, and JSASS, International Electric Propulsion Conference, 19th, Colorado Springs, CO, May 11–13, 1987, 10
Circi, C., & Teofilatto, P. 2001, Celest. Mech. & Dyn. Astro., 79, 41
Farquhar, R. W., & Kamel, A. A. 1973, Celestial Mechanics, 7, 458
Franco, B. Z., et al. 2004, ESA Contract Contract Number: 18147/04/NL/MV
Gómez, G., Jorba, A., Masdemont, J., & Simó, C. 1993, Celest. Mech. & Dyn. Astro., 56, 541
Gómez, G., Jorba, A., Masdemont, J., & Simó, C. 1998, Acta Astronautica, 43, 493
Gómez, G., Llibre, J., Martínez, R., & Simó, C. 2001a, Dynamics and Mission Design Near Libation Point Orbits, Vol. 1, Fundamentals: The Case of Collinear Libration Points (Singapore: World Scientific)
Gómez, G., Jorba, A., Masdemont, J., & Simó, C. 2001b, Dynamics and Mission Design Near Libration Point Orbits, Vol. 3, Advanced Methods for Collinear Points (Singapore: World Scientific)
Gómez, G., et al. 2004, Nonlinearity, 17, 1571
Hou, X.-Y., & Liu, L. 2008, Chin. Astron. Astrophys., 32, 73
Koon, W. S., et al. 2000, Chaos, 10, 427
Koon, W. S., et al. 2001, Celest. Mech. & Dyn. Astro., 81, 63
Liu, C.-B., Hou, X.-Y., & Liu, L. 2007, Advances in Space Research, 40, 76
Llibre, J., Martinez, R. & Simó, C. 1985, Journal of Differential Equations, 58, 104
Lo, M., et al. 1998, AIAA Astrodynamics Conference, August, 1998, Boston, MA. Paper No. 98-4468
Lo, M. W. 2002, IEEE Aerospace Conference Proceedings, Vols. 1–7, 3543
Lo, M. W., & Chung, M. K. 2002, AIAA, 4718
Szebehely, V. 1967, Theory of Orbits (New York: Academic Press)